Christoph PEUKERT[1*], Patrick PÖHLMANN[1],
Marcel MERX[1], Georg Constantin FISCHER[1],
Jens MÜLLER[1], Steffen IHLENFELDT[1,2]

SIMULATION-BASED ANALYSIS OF THE MODAL CONTROL OF BALL SCREW DRIVEN FEED AXES

Feed axes of machine tools often include more sensors and actuators than needed for basic motion generation. In such over-actuated systems, actuator control is typically implemented in an independent manner, without explicit consideration of the dynamic interactions between individual control loops. The performance of such decentralised control schemes is often limited. Modal decoupling enables the system to be separated into individual vibration modes, each controlled independently. The advantage of modal control lies in its ability to simplify the control of complex systems by reducing them to multiple independent single-input, single-output systems. Each control loop corresponds to a specific vibration mode, and its control law can be designed to meet the desired performance requirements. This study presents a simulation-based analysis of modal control applied to feed axes equipped with a ball screw. Two over-actuated configurations are examined. The first consists of a ball screw driven by a single motor, with an optional active damping device attached to the slide. The second configuration features a ball screw driven by two motors, one mounted on each side. Applying modal control increases the position-control bandwidth by up to 60 % when using an active damping device, and by up to 20 % for a dual-motor ball screw axis.

1. INTRODUCTION

High-speed metal cutting machines require high feed dynamics, which can be achieved by increasing the force or torque of the feed drive. For this purpose, multiple drives per axis are applied. The gantry architecture, which implements the principle of "Drive at the Center of Gravity" [1] and prevents the slide from yawing, represents a solution for constructively increasing the feed dynamics [2]. Moreover, two motors can be connected to both ends of a ball screw to drive the slide. This so-called "both-side drive" [3], also referred to as the "Zero Gap Drive System" [4], allows for a thermally symmetrical machine design and enhances

both motion dynamics and accuracy. To achieve high feed dynamics, active damping devices (ADD) equipped with proof-mass actuators are employed to dampen structural modes and increase the chatter-free cutting depth [5]. These systems can be easily integrated into machine tools without any design modifications being required.

As an essential component of machine tools, the dynamic properties of the feed drive system have a significant influence on machining performance. For machine tools with short and medium axis lengths, backlash-free, preloaded ball screws are the preferred drive system. Ball screw drives (BSD) are characterised by high accuracy, load capacity and dynamics [6]. When high positioning accuracy is required, a linear encoder is used in addition to the rotary encoder to directly measure the slide position. In this case, wear and temperature-induced changes in the drive mechanism as well as inaccuracies in the transmission elements – such as spindle lead errors – can be eliminated. In this drive configuration, the actuator and sensor are not collocated, as the linear encoder and the motor are not in the same physical location. In addition, the BSD dynamics (i.e. eigenfrequencies and modes) vary according to the position of the slide [7]. The achievable bandwidth of the position loop of BSD feed axes with conventional P-PI position-velocity cascade control (industrial standard) is limited by structural vibrations originating from the axial and torsional modes of the mechanical transmission elements [8]. In [9], a friction-based actuator is used to suppress the axial vibration mode of a BSD. To increase the bandwidth of the position loop of BSD axes, several control solutions have been proposed. In [10] for example, a cascaded feedback control is presented consisting of a weakly set motor velocity controller, a disturbance observer loop and a superimposed PD position controller. In [11], axial vibrations are modelled and actively compensated for in the control law, which enables the realisation of a high positioning bandwidth. To improve the dynamics of a BSD the P position controller of the cascade control can be substituted with a sliding mode controller [12]. In [13], a modal characteristic modifier is presented that employs a combination of peak and notch filters to reshape the plant dynamics into a virtually collocated system, thereby avoiding control spillover.

This paper discusses the control of BSD feed axes in modal space. Two modal control strategies have been developed. The effectiveness of these approaches is demonstrated through simulations involving an axis with BSD and a proof-mass actuator, as well as a BSD driven by two servomotors. By applying the modal transformation, the dynamics of the feed axis are decoupled, allowing the system's eigenmodes to be controlled individually [14]. The modal control (MC) is particularly advantageous for axes with more sensors, drives or actuators than is necessary for generating and capturing feed motion [15].

2. MODAL DECOUPLING AND MODAL CONTROL APPROACH

The mechanical structure of a motion system shown in Fig. 1, left, can be expressed as a coupled system of ordinary differential equations:

$$M\ddot{q} + D\dot{q} + Kq = f, \tag{1}$$

where M, D and K are the mass, damping and stiffness matrix respectively. The dynamic system can be decoupled using the modal transformation. The eigenvector matrix Φ of the

matrix $M^{-1}K$ forms the transformation between physical q and modal coordinates ξ:

$$q = \Phi\xi. \tag{2}$$

Substituting Eq. (2) into Eq. (1) and normalising the eigenvectors such that the modal mass matrix becomes the identity matrix transforms the equation of motion into its modal form:

$$\ddot{\xi} + \Delta\dot{\xi} + \Lambda\xi = \tau \quad \text{with} \quad \tau = \Phi^{\mathrm{T}}f. \tag{3}$$

The matrix of the eigenvalues Λ consists of main diagonal entries only. Assuming the matrix of modal damping ratios, denoted by Δ, can be approximated as diagonal, Eq. (3) decouples into N independent scalar equations:

$$\ddot{\xi}_i + 2\delta_i\dot{\xi}_i + \omega_i^2\xi_i = \tau_i, \quad i = 1 \dots N, \tag{4}$$

where δ_i and ω_i are the damping ratio and the eigenfrequency of the ith mode, respectively. The dynamics of the system are now represented by the transfer function matrix $G_{\mathrm{mod}}(j\omega)$ containing N decoupled single-mass oscillators in modal space, as shown in Fig. 1, right. The modal control approach utilises the independence of the modal systems from Eq. (4). An independent control law $R_{\mathrm{mod},i}$ can be formulated for each modal system [16]:

$$\tau_{\mathrm{C},i} = R_{\mathrm{mod},i}(j\omega)\xi_{\mathrm{C},i}, \quad i = 1 \dots m_{\mathrm{C}}. \tag{5}$$

The modal loads τ_{C} are calculated for a limited number of controlled modes m_{C}. The modal coordinates ξ_{C} and the actuator forces f_{A} are calculated using the modal filter Ψ^{T} [17] and the modal synthesizer Θ with q_{S} representing the measured coordinates:

$$\xi_{\mathrm{C}} = \Psi^{\mathrm{T}}q_{\mathrm{S}} \quad \text{and} \quad f_{\mathrm{A}} = \Theta\tau_{\mathrm{C}} \quad \text{with} \quad \Psi^{\mathrm{T}} = (\Phi_{\mathrm{CS}})^{-1} \quad \text{and} \quad \Theta = (\Phi_{\mathrm{CA}}^{\mathrm{T}})^{-1}, \tag{6}$$

where Φ_{CS} and Φ_{CA} are submatrices of Φ. Φ_{CS} includes only the columns corresponding to the controlled modes ξ_{C} and the rows associated with the measured coordinates q_{s}. In Φ_{CA}, the rows corresponding to the actuator forces f_{A} are selected.
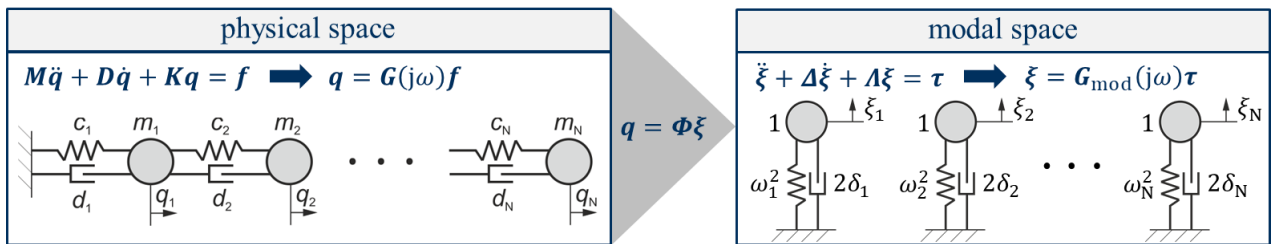

Fig. 1. Modal decoupling technique

3. MODEL APPROACH

The test rig depicted in Fig. 2 was designed and built in order to assess the potential of modal control for over-actuated axes with BSD. This study focuses exclusively on simulation-based investigations. The model specifications are derived from this test rig. The feed axis

analysed consists of a spindle with a diameter of $d_{sp} = 32\,\text{mm}$, a total length of $l_{sp} = 1752\,\text{mm}$, and a lead of $h_{sp} = 32\,\text{mm}$, driven by servomotors with an inertia of $J_{Mot} = 0.00085\,\text{kgm}^2$. The mass of the slide is $m_{slide} = 130\,\text{kg}$. To ensure consistency in units, the rotary encoder signal was converted into an equivalent slide displacement, and the motor torque into an equivalent force.
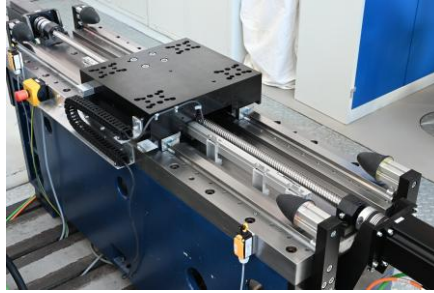

Fig. 2. Feed axis with a ball screw driven by dual motors, serving as the basis for the derived models

3.1. FINITE ELEMENT MODEL

The main components of the BSD feed axis are modelled in ANSYS®, where the ball screw spindle and motor rotors are meshed with beam elements. Remote points were created for the subsequent coupling of subsystems. In order to analyse the feed axis behaviour at various slide positions, the modal parameters of the frame (comprising the spindle, motors and couplings) as well as those of the slide were exported individually from ANSYS®. Fig. 3 provides an overview of the exported submodels. The frame's modal matrices include eigenmodes with frequencies up to 2 kHz, while those of the slide extend up to 10 kHz.
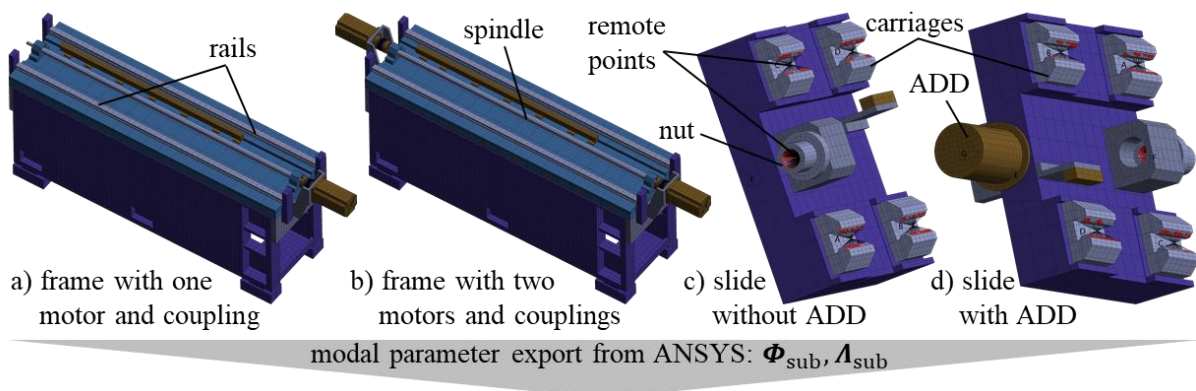

Fig. 3. Submodels exported from ANSYS for different simulation scenarios

In this paper, three axis configurations are investigated. The first configuration is a standard BSD (Fig.°3a+c and Fig. 4a). The second configuration extends the first by adding an additional ADD mounted on the slide (Fig.°3a+d and Fig.°9). The third configuration features two motors and couplings attached to the spindle (Fig.°3b+c and Fig. 14a). To couple

the systems in MATLAB$^{®}$, the additional stiffness between the carriages and the rails of the guiding system, and between the nut and the spindle, must be taken into account. Modelling the stiffness conditions at the contact between ball and groove of the BSD is essential for the representation of the dynamic behaviour of the axis. Since the remote points of the ball screw and the nut coincide, and the spindle is aligned along the y-direction, the stiffness matrix K_{NS} between the spindle and the nut has the form [18]:

$$K_{NS} = \begin{bmatrix} \widetilde{K}_{NS} & -\widetilde{K}_{NS} \\ -\widetilde{K}_{NS} & \widetilde{K}_{NS} \end{bmatrix} \text{ with}$$

$$\widetilde{K}_{NS} = \begin{bmatrix} k_{rad} & 0 & 0 & 0 & 0 & 0 \\ 0 & k_{ax} & 0 & 0 & \left(\dfrac{h_{sp}}{2\pi}\right) \cdot k_{ax} & 0 \\ 0 & 0 & k_{rad} & 0 & 0 & 0 \\ 0 & 0 & 0 & k_{rot} & 0 & 0 \\ 0 & \left(\dfrac{h_{sp}}{2\pi}\right) \cdot k_{ax} & 0 & 0 & \left(\dfrac{h_{sp}}{2\pi}\right)^2 \cdot k_{ax} & 0 \\ 0 & 0 & 0 & 0 & 0 & k_{rot} \end{bmatrix}, \tag{7}$$

where k_{ax}, k_{rad} and k_{rot} are the axial, radial and rotational stiffness of the spindle-nut contact respectively. The modal subsystem matrices are assembled into new block-diagonal matrices:

$$\begin{pmatrix} \ddot{\xi}_{sub,1} \\ \ddot{\xi}_{sub,2} \end{pmatrix} + \underbrace{\begin{bmatrix} \Lambda_{sub,1} & 0 \\ 0 & \Lambda_{sub,2} \end{bmatrix}}_{\Lambda_{12}} \begin{pmatrix} \xi_{sub,1} \\ \xi_{sub,2} \end{pmatrix} = \begin{pmatrix} \tau_{sub,1} \\ \tau_{sub,2} \end{pmatrix} \text{ and } \Phi_{12} = \begin{bmatrix} \Phi_{sub,1} & 0 \\ 0 & \Phi_{sub,2} \end{bmatrix}. \tag{8}$$

The coupling stiffness K_{add}, which incorporates the stiffness of the guiding system and the spindle-nut contact, is transformed into the modal space via the modal matrix Φ_{12}, and added to the eigenvalue matrix Λ_{12}:

$$\widetilde{\Lambda}_{12} = \Lambda_{12} + \Phi_{12}^T K_{add} \Phi_{12}. \tag{9}$$

The resulting matrix $\widetilde{\Lambda}_{12}$ is no longer diagonal. To re-diagonalise the system, the eigenvalue problem of the updated system is solved again, yielding the new modal matrix $\widetilde{\Phi}_{12}$. The eigenvalue and eigenvector matrices of the composed system are then obtained as:

$$\Lambda_{comp} = \widetilde{\Phi}_{12}^T \widetilde{\Lambda}_{12} \widetilde{\Phi}_{12} \text{ and } \Phi_{comp} = \Phi_{12} \widetilde{\Phi}_{12}. \tag{10}$$

Finally, the modal damping matrix of the composed system Δ_{comp} is defined based on modal damping ratios. The synthesised modal system consists of m modes and N coordinates. Since only m modes are considered, the system is already in a reduced form (indices for the composed system are omitted below):

$$\ddot{\xi}^{[m\times 1]} + \Delta^{[m\times m]\dagger} \dot{\xi}^{[m\times 1]} + \Lambda^{[m\times m]} \xi^{[m\times 1]} = (\Phi^T)^{[m\times N]} f^{[N\times 1]}. \tag{11}$$

[†] The dimensions of the respective matrix or vector are provided in square brackets.

3.2. REDUCED STATE-SPACE MODEL

The system defined in Eq. (11) is used to formulate the modal state-space representation:

$$\dot{x} = \begin{pmatrix} \dot{\xi} \\ \ddot{\xi} \end{pmatrix} = Ax + Bf \quad \text{and} \quad y = Cx \quad \text{with} \quad A^{[2m\times2m]} = \begin{bmatrix} \mathbf{0}^{[m\times m]} & I^{[m\times m]} \\ -\Lambda^{[m\times m]} & -\Delta^{[m\times m]} \end{bmatrix},$$

$$B^{[2m\times N]} = \begin{bmatrix} \mathbf{0}^{[m\times N]} \\ (\boldsymbol{\Phi}^{\mathrm{T}})^{[m\times N]} \end{bmatrix} \quad \text{and} \quad C^{[2N\times2m]} = \begin{bmatrix} \boldsymbol{\Phi}^{[N\times m]} & \mathbf{0}^{[N\times m]} \\ \mathbf{0}^{[N\times m]} & \boldsymbol{\Phi}^{[N\times m]} \end{bmatrix}, \quad (12)$$

where A, B and C are the state, input and output matrix respectively. For the transfer function matrix that is used for modal control analysis, only the input-output behaviour at several coordinates is required. Selection matrices are therefore introduced, with n_S representing the number of sensors and n_A the number of actuators. The coordinates at which loads are applied are selected with $S_A^{[N\times n_A]}$ and the coordinates at which sensors are located with $S_S^{[n_S\times2N]}$. Thus, the load and sensor vector become $f = S_A^{[N\times n_A]}f_A$ and $y_S = S_S^{[n_S\times2N]}y$ respectively. The reduced state space system results in:

$$\dot{x} = \begin{pmatrix} \dot{\xi} \\ \ddot{\xi} \end{pmatrix} = Ax + B_{\mathrm{red}}f_A \quad \text{and} \quad y_s = C_{\mathrm{red}}x \quad \text{with} \quad B_{\mathrm{red}}^{[2m\times n_A]} = B^{[2m\times N]}S_A^{[N\times n_A]}, \quad (13)$$

$$C_{\mathrm{red}}^{[n_S\times2m]} = S_S^{[n_S\times2N]}C^{[2N\times2m]} \quad \text{and} \quad S_S^{[n_S\times2N]} = \begin{bmatrix} S_{\mathrm{pos}}^{[n_{S,\mathrm{pos}}\times N]} & S_{\mathrm{vel}}^{[n_{S,\mathrm{vel}}\times N]} \end{bmatrix}.$$

If the sensor outputs y_S are positions, $S_{\mathrm{vel}}^{[n_S\times N]}$ is set to the zero matrix, and if the outputs are velocities, $S_{\mathrm{pos}}^{[n_S\times N]}$ is set to the zero matrix.

Taking the Laplace transform of Eq. (13) and assuming zero initial conditions, the transfer function matrix $G_{\mathrm{mech}}(s)$ of the mechanics is obtained as follows:

$$y_S^{[n_S\times1]} = \underbrace{C_{\mathrm{red}}^{[n_S\times2m]}\left(sI - A^{[2m\times2m]}\right)^{-1}B_{\mathrm{red}}^{[2m\times n_A]}}_{G_{\mathrm{mech}}^{[n_S\times n_A]}(s)} f_A^{[n_A\times1]}. \quad (14)$$

To assess the accuracy of the reduced transfer function matrix G_{mech}, the coupling of the subsystems was also performed in ANSYS®. The resulting frequency response comparison confirms that neglecting higher-order eigenmodes has only a negligible influence on the system behaviour within the frequency range of interest. The transfer functions of the current controller (bandwidth: 800 Hz, deadtime: 125 µs) and the mechanical system $G_{\mathrm{mech}}^{[n_S\times n_A]}$ form the plant $G^{[n_S\times n_A]}$, which is used for the following analyses in the frequency domain. The sampling time of the controllers is 250 µs.

3.3. EVALUATION OF CONTROL PERFORMANCE

As the feed axis configurations represent multi-variable systems, the stability analysis is performed according to the Nyquist criterion using the eigenvalues $\lambda_i(\mathrm{j}\omega)$ of the matrix GR and the determinant of the return difference operator $(I + GR)$ [19]. Here, R represents the

matrix of the controller transfer functions. All controllers will be set so that there is at least a gain margin of 2. The sensitivity S and complementary sensitivity function T are calculated in order to compare the control strategies. S is the closed-loop transfer function from the output disturbances to the outputs, while T is the closed-loop transfer function from the reference signals to the outputs. These frequency response functions (FRFs) are defined as:

$$S = (I + GR)^{-1}, \quad T = SGR. \tag{15}$$

To achieve good control performance – such as good disturbance rejection, reference tracking, and mitigation of measurement noise – for the investigated feed axis configurations, the maximum peaks of the sensitivity M_S and complementary sensitivity functions of the velocity $M_{T,vel}$ and position loop $M_{T,pos}$ are defined as follows [20]:

$$M_S = \max_\omega |S| \le 2.25 \,, \qquad M_{T,vel} = \max_\omega |T| \le 1.25 \,, \qquad M_{T,pos} = \max_\omega |T| \le 1. \tag{16}$$

4. MODAL CONTROL OF A BALL SCREW AXIS DRIVEN BY ONE MOTOR

Firstly, the standard axis configuration of machine tools, consisting of a ball screw, a servomotor ($M_{Mot,1}$) including a rotary encoder ($y_{rot,1}$) and a linear encoder for detecting the slide position y_{lin} is analysed (see Fig. 4a). Fig. 4b shows the control-relevant mode shape of the feed axis (axial mode): a rotation φ_y of the spindle, the coupling and the motor rotor, which is coupled with an antiphase translational vibration of the slide.
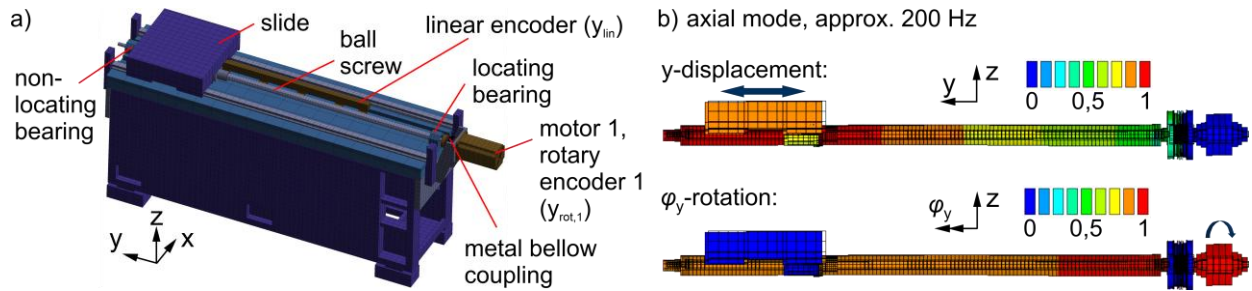

Fig. 4. Feed axis with a ball screw driven by one motor (slide at Pos. 3): FE-model (a) and first relevant eigenform (b)

4.1. MODAL DECOMPOSITION OF THE FEED AXIS WITH ONE SERVOMOTOR

The matrix of FRFs of the feed axis with a single motor is obtained by:

$$\dot{\boldsymbol{y}} = \begin{pmatrix} \dot{y}_{rot,1} \\ \dot{y}_{lin} \end{pmatrix} = \underbrace{\begin{pmatrix} G_{11}(j\omega) \\ G_{21}(j\omega) \end{pmatrix}}_{\boldsymbol{G}(j\omega)} \cdot F_{Mot,1}. \tag{17}$$

Figure 5a+b depicts the plants in physical coordinates for three slide positions. The spindle section in the force-flow changes according to the slide position. This reduces the

resonance frequency from approx. 230 Hz (slide near locating bearing: Pos. 1) to approx. 195 Hz (slide near non locating bearing: Pos. 3, see Fig. 4). The second resonance occurs at around 730 Hz and is attributed to the first torsional mode. In the following analyses, it is assumed the slide is in the middle position (Pos. 2). The system's dynamic response in modal space is given by:

$$\begin{pmatrix} \dot{\xi}_{C,1} \\ \dot{\xi}_{C,2} \end{pmatrix} = \underbrace{\boldsymbol{\Psi}_{[2\times2]}^{T} \cdot \boldsymbol{G}(j\omega) \cdot \boldsymbol{\theta}_{[1\times2]}}_{\boldsymbol{G}_{\mathrm{mod}}(j\omega)} \cdot \begin{pmatrix} \tau_1 \\ \tau_2 \end{pmatrix}, \quad \boldsymbol{\theta}_{[1\times2]} = (w_1 \quad w_2), \tag{18}$$

whereby the modal filter $\boldsymbol{\Psi}_{[2\times2]}^{T}$ considers the rigid body motion and the axial eigenmode only. As two sensors are available, two modes can be decoupled internally with the modal filter. However, since the number of actuators n_A is smaller than the number of sensors n_S, the system is externally coupled. In such case, the actual forces can be synthesised from the modal control forces by computing the pseudo-inverse of ($\boldsymbol{\Phi}_{CA}^{T}$). However, pseudo-inverses are not exact inverses, so errors are to be expected [21]. The modal synthesiser $\boldsymbol{\theta}_{[1\times2]}$ in Eq. (18) used for this configuration is simply a weighted sum of the outputs of the modal controllers. The phase curve for the non-collocated situation (G_{21} in Fig. 5b) illustrates that the system is prone to instability when the linear encoder signal is used in a conventional velocity control loop. However, applying the modal transformation allows the rigid body motion to be separated internally from the first axial mode, as shown in Fig. 5c+d. Until 300 Hz, $G_{\mathrm{mod},11}$ exhibits behaviour similar to that of a first-order integrator because the first mode represents the rigid-body motion. A phase delay, as with the sole use of the linear encoder, is not to be recognised. The torsional mode at approx. 730 Hz cannot be decoupled. In this configuration, there is an external coupling due to the off-diagonal transfer functions having non-negligible magnitudes, as $G_{\mathrm{mod},11} = G_{\mathrm{mod},12}$ and $G_{\mathrm{mod},22} = G_{\mathrm{mod},21}$.
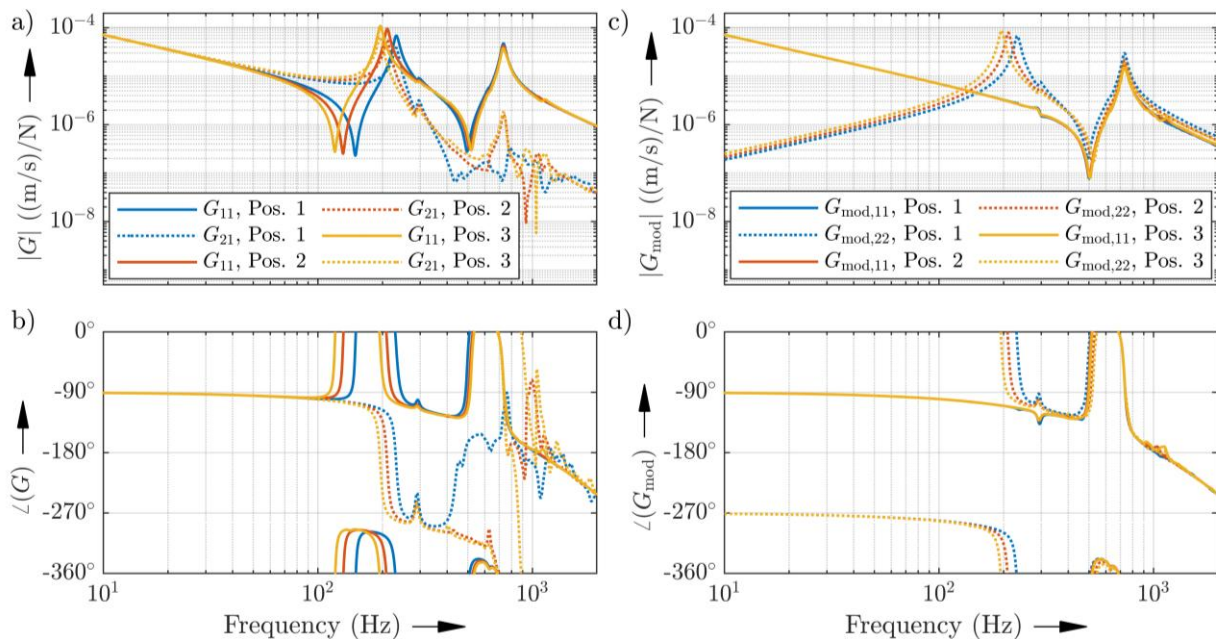

Fig. 5. Feed axis FRFs with one motor at three slide positions: without modal decoupling (a+b) and with decoupling for $w_1 = w_2 = 1$ (c+d)

4.2. CONTROL DESIGN OF THE FEED AXIS WITH ONE MOTOR WITHOUT ADD

The analysed control strategies for the ball screw feed axis with one motor are depicted in Fig. 6. Achieving high positioning accuracy for the rigid body motion requires a P-PI loop as the first modal controller $R_{1,\text{mod}}$ (Fig. 6b), which can be tuned from the inside outwards much like conventional control loops. The proposed modal control concept only applies a modal transformation to the actual velocity signals. A modal transformation in the position control loop would lead to a reduction in static positioning accuracy due to the incorporation of the rotary encoder signal. The MC is compared with a conventional decentralised control (DC) approach for electromechanical axes, where the rotary encoder signal is fed back into the velocity control loop and the linear encoder signal is used for position control (Fig. 6a). For the DC, the indirect acquisition of the actual velocity of the slide via the rotary encoder is advantageous because the amplitudes of the slide vibrations only affect the measurement signal in the form of a negligible torsional excitation of the ball screw [23].
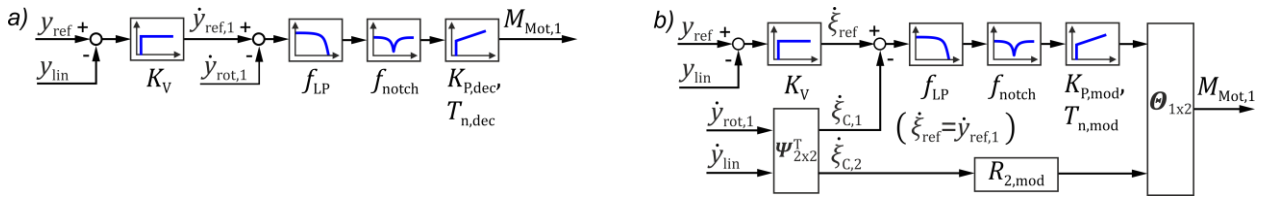

Fig. 6. Control strategies for the ball screw feed axis with one motor: DC (a) and MC (b)

Both the decentralised controller R_{dec} and the first modal controller $R_{1,\text{mod}}$ have the same cascaded control configuration. A notch filter set to 730 Hz was incorporated into both control schemes to prevent excitation of the first torsional resonance. The Nyquist plots of the open velocity loops for the control variants are shown in Fig. 7. It should be mentioned that the determinate of $(I + GR)$ does not encircle the origin in the part of the curve not shown. In principle, high velocity loop gains of $R_{1,\text{mod}}$ can be achieved by using the modal approach (Fig. 7 and Fig. 8a+b). However, high resonance peaks were observed for both the reference response (Fig. 8c) and the slide disturbance response represented by the matrix $\boldsymbol{SG}$ (Fig. 8d).
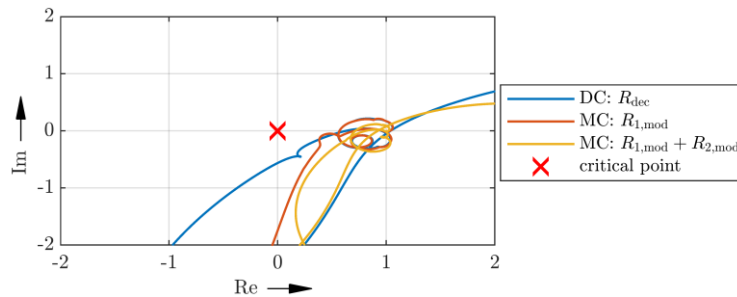

Fig. 7. BSD feed axis driven by one motor, velocity loop: Nyquist plot of $\det(I + \boldsymbol{GR})$

Activating the second modal controller $R_{2,\text{mod}}$, a P-controller with high-pass filter, enables attenuation of the resonances. As there is only one actuator, interaction between the modal control loops is unavoidable and the bandwidth of the position control loop cannot be increased. Thus, the advantage of simple parameterisation due to modal decoupling cannot be

realised without adapting the control structure further. Therefore, modal control offers no significant benefit to this configuration.
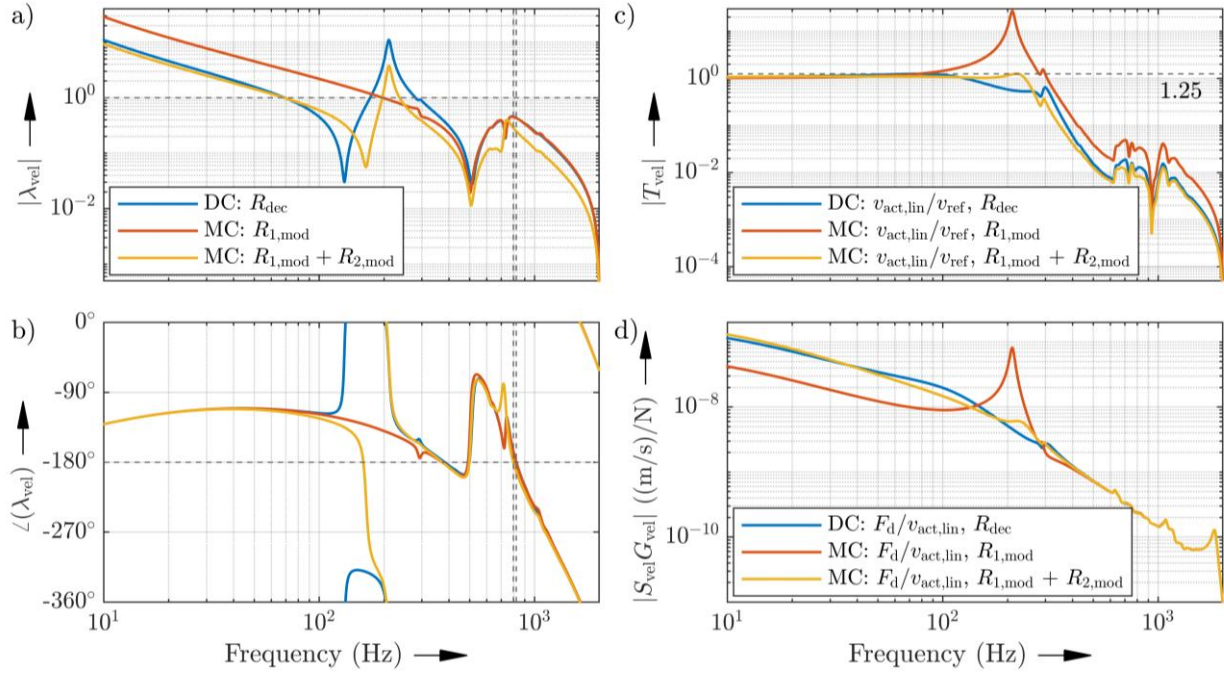

Fig. 8. BSD with one motor, velocity loop: eigenvalues (a+b), complementary sensitivity (c), disturbance response (d)

4.3. CONTROL DESIGN OF THE FEED AXIS WITH ONE MOTOR AND ONE ADD

This section examines the MC of a BSD axis equipped with one motor and an additional ADD, which is mounted on the slide (see Fig. 9). The ADD is a system comprising of a proof-mass actuator, an accelerometer, and a control unit. The internal controller is not required for implementing MC. Proof-mass actuators generate forces by accelerating a suspended mass that is mechanically coupled to the main structure, as illustrated in Fig. 9, right. The actuator behaves as an ideal force generator at frequencies above its suspension frequency. Its operating bandwidth ranges from 25 to 2000 Hz. The specific proof-mass actuator considered in this study has a moving mass of $m_{ADD} = 2.2$ kg and a resonant frequency of 8.4 Hz.
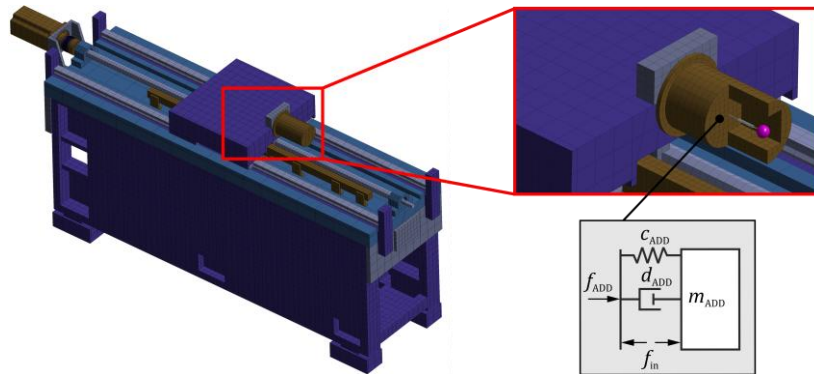

Fig. 9. BSD feed axis with one motor and one ADD

For this system, the modal synthesizer can be obtained by inverting the matrix ($\boldsymbol{\Phi}_{\mathrm{CA}}^{\mathrm{T}}$):

$$\begin{pmatrix} \dot{\xi}_{\mathrm{C},1} \\ \dot{\xi}_{\mathrm{C},2} \end{pmatrix} = \underbrace{\boldsymbol{\Psi}_{[2\times2]}^{\mathrm{T}} \cdot \boldsymbol{G}(\mathrm{j}\omega) \cdot \boldsymbol{\theta}_{[2\times2]}}_{\boldsymbol{G}_{\mathrm{mod}}(\mathrm{j}\omega)} \cdot \begin{pmatrix} \tau_1 \\ \tau_2 \end{pmatrix}, \quad \boldsymbol{\theta}_{[2\times2]} = (\boldsymbol{\Phi}_{\mathrm{CA}}^{\mathrm{T}})^{-1}. \tag{19}$$

The modal FRFs of the main diagonals of G_{mod} are very similar to Fig. 5c+d and are thus not shown. However, since the rigid body motion and the axial mode can be decoupled effectively, the FRFs of the off-diagonals of G_{mod} have negligible amplitudes. The modal and decentralised control strategies are illustrated in Fig 10. When operated at or below the natural frequency of the inertial actuator, the stroke of the reaction mass of the ADD becomes very large and high stress amplitudes result. For this reason, the controllers $R_{2,\mathrm{dec}}$ and $R_{2,\mathrm{mod}}$ employ a band-pass filter with gain, and the modal control concept incorporates further high and low-pass filtering. In the second modal loop, the two modes are decoupled by using both actuators. The loads calculated for the motor from both loops are added (see Fig. 10b).
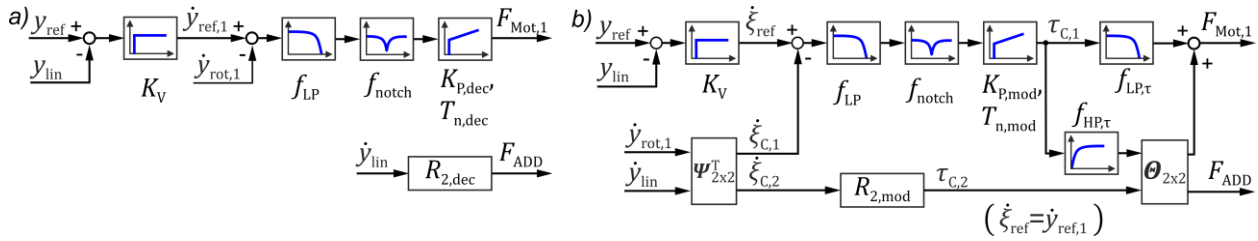

Fig. 10. Control strategies for the ball screw feed axis with one motor and one ADD

The Nyquist plot in Fig. 11 shows that higher gains can be set in the modal velocity loops, while simultaneously achieving higher gain and phase margins. Due to the coupling of the control loops, the gains in the DC cannot be increased any further, as this would result in insufficient stability margins.
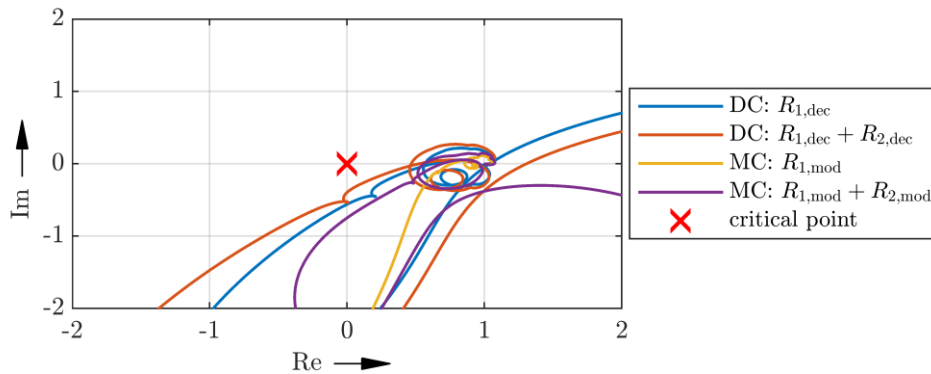

Fig. 11. Feed axis with one motor and one ADD, velocity loop: Nyquist plot of $\det(\boldsymbol{I} + \boldsymbol{GR})$

Significantly improved reference tracking can be achieved by applying the MC (see Fig. 12a). Furthermore, the response to disturbances on the slide – for example, those resulting from a process load – is much better than that observed with the DC, as shown in Fig. 12b.
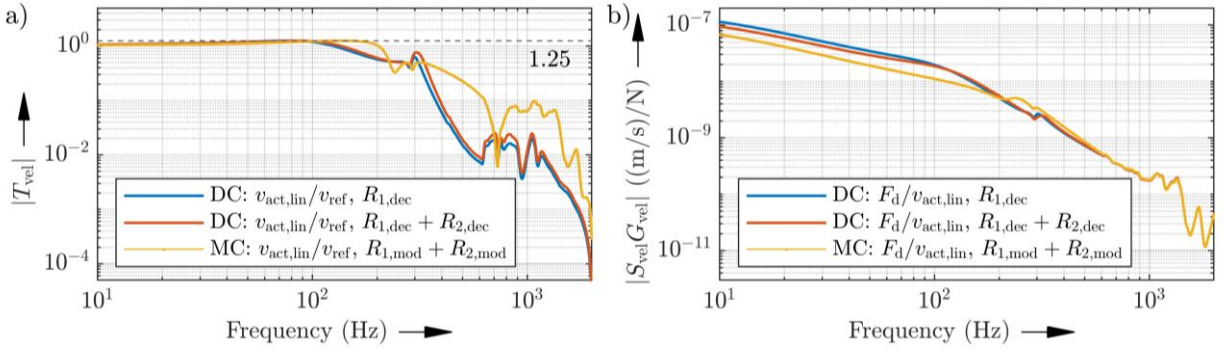
Fig. 12. Velocity loop: complementary sensitivity function (a) and disturbance response (b)

Activating the decentralised controller $R_{2,\mathrm{dec}}$ for the ADD results in a slightly higher velocity gain factor K_v for the position controller. Compared to the DC approach, the MC's K_v factor is 45 % higher, and the control bandwidth can be expanded by 60 % (see Fig. 13a). Noise or disturbances at the linear encoder $y_{\mathrm{n,lin}}$ can be attenuated more effectively at low frequencies using MC. However, the MC's noise suppression deteriorates at frequencies above 100 Hz, as illustrated in Fig. 13b.
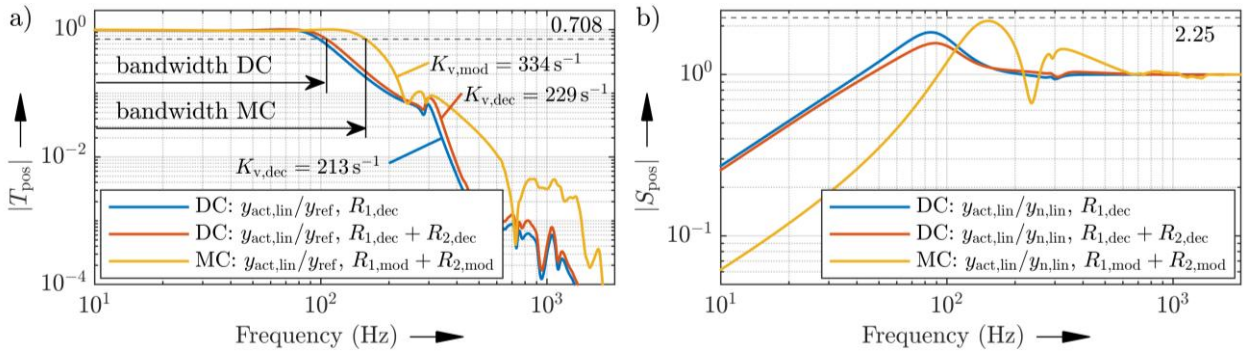

Fig. 13. Position loop: complementary sensitivity function (a) and sensitivity function (b)

The proposed modal control approach for BSD, with the addition of an ADD, significantly improves mechanical disturbance rejection and delivers better dynamic positioning accuracy than a conventional controller. Applying the MC of the BSD axis with inertial actuators for active vibration damping can considerably minimise the impact on the position control of the feed drives. However, the use of an additional ADD has the disadvantage that additional damping energy is required.

5. MODAL CONTROL OF A BALL SCREW AXIS DRIVEN BY TWO MOTORS

For this analysis, a second, identical motor is attached to the spindle, as can be seen in the depicted FE-model in Fig. 14a. Therefore, the total inertia is increased and the driving torque is doubled. The axial and first torsional natural frequencies are shifted to lower values compared to the single-sided drive, as shown in Fig. 15a+b. The corresponding mode shapes are illustrated in Fig. 14b+c.
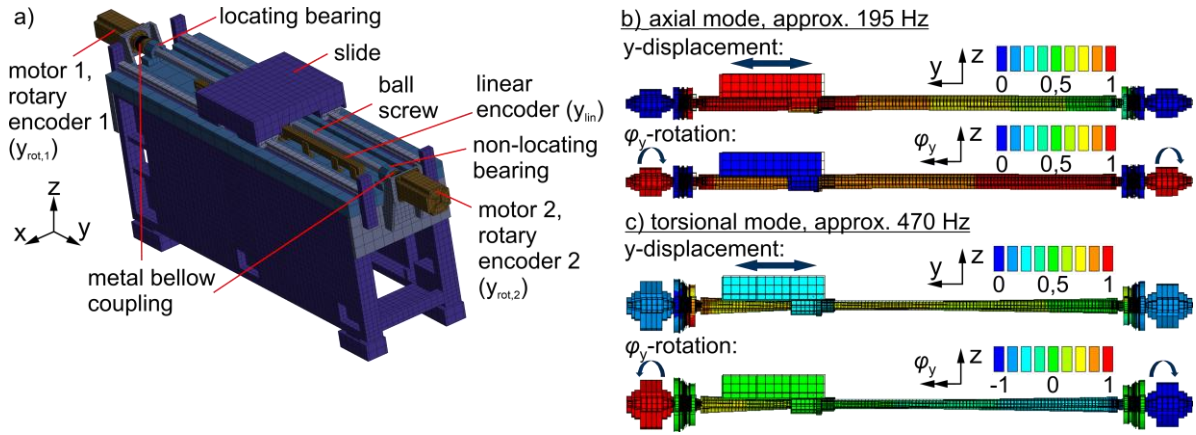
Fig. 14. Feed axis with a ball screw driven by two motors: FE-model (a) and relevant eigenforms (b+c)

The dynamics of the axis with a ball screw driven by two motors are given by:

$$\dot{\boldsymbol{y}} = \begin{pmatrix} \dot{y}_{\text{rot},1} \\ \dot{y}_{\text{rot},2} \\ \dot{y}_{\text{lin}} \end{pmatrix} = \underbrace{\begin{pmatrix} G_{11}(\mathrm{j}\omega) & G_{12}(\mathrm{j}\omega) \\ G_{21}(\mathrm{j}\omega) & G_{22}(\mathrm{j}\omega) \\ G_{31}(\mathrm{j}\omega) & G_{32}(\mathrm{j}\omega) \end{pmatrix}}_{\boldsymbol{G}(\mathrm{j}\omega)} \cdot \begin{pmatrix} F_{\text{Mot},1} \\ F_{\text{Mot},2} \end{pmatrix}. \tag{20}$$

In this configuration, there is an interaction between the motors. The torsional resonance limits the stability margins and the achievable positioning bandwidth. Only the signals of the rotary encoders are considered for the modal decoupling. Using the modal filter $\boldsymbol{\Psi}^{\mathrm{T}}_{[2x2]}$ and the modal synthesizer $\boldsymbol{\theta}_{[2\times2]}$, the modal system can be obtained from the physical system $\boldsymbol{G}_{[2\times2]}$ (without linear encoder output):

$$\begin{pmatrix} \dot{\xi}_{C,1+2} \\ \dot{\xi}_{C,3} \end{pmatrix} = \underbrace{\boldsymbol{\Psi}^{\mathrm{T}}_{[2x2]} \cdot \boldsymbol{G}_{[2\times2]}(\mathrm{j}\omega) \cdot \boldsymbol{\theta}_{[2\times2]}}_{\boldsymbol{G}_{\text{mod}}(\mathrm{j}\omega)} \cdot \begin{pmatrix} \tau_{1+2} \\ \tau_3 \end{pmatrix}, \quad \boldsymbol{\theta}_{[2\times2]} = \left(\boldsymbol{\Phi}^{[2\times2]}_{\text{CA}}\right)^{-\mathrm{T}}. \tag{21}$$
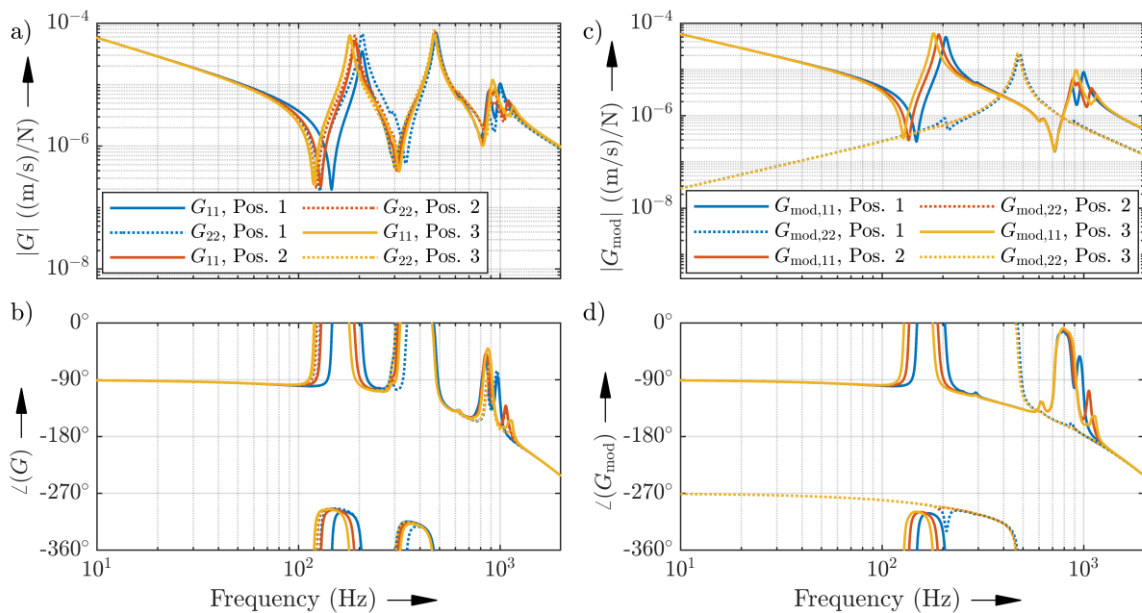

Fig. 15. Feed axis FRFs with two motors at three slide positions: no modal decoupling (a+b) vs. with decoupling (c+d)

As can be seen from Fig. 15c+d, the torsional mode can be separated from the rigid body motion and the axial mode. This is advantageous for the velocity loop control design, as it allows for the development of individual control loops.

5.1. CONTROL STRATEGY

In contrast to the controller proposed in [3], the DC scheme uses two position controllers, whereby the signal from the linear encoder and the rotary encoder are fed back (see Fig. 16a). In this way, tensioning of the spindle by the two integral components of the velocity control loops can be avoided. A notch filter at approximately 470 Hz is used for the DC, but this is not required for the MC strategy. The MC utilises the modal transformations outlined in Eq. (21) to control the torsional mode independently of the other modes (Fig. 16b). The first modal controller, $R_{12,\mathrm{mod}}$, is also a P-PI controller that is primarily tuned to the rigid body motion and the axial mode. The second modal controller, $R_{3,\mathrm{mod}}$, is a P controller with a high-pass filter, that is tuned to dampen the torsional resonance.
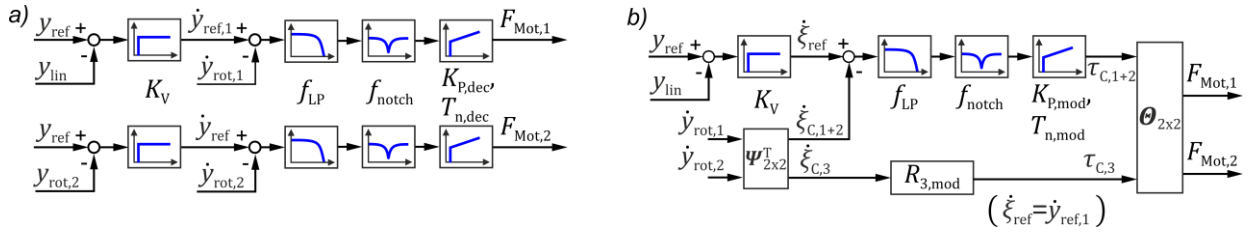

Fig. 16. Control strategies for the ball screw feed axis with two motors: DC (a) and MC (b)

5.2 CONTROL DESIGN

Fig. 17 compares DC with MC using one or both active modal controllers. The first modal controller can achieve higher gains than a decentralised control system. This enhancement is accomplished by eliminating the adverse impact of the torsional mode on the closed loop stability. Similar stability margins to those in DC can be achieved by setting higher gains for the first modal velocity controller. As can be seen from Fig. 17, activating the second modal controller, $R_{3,\mathrm{mod}}$, does not affect the stability margins of the system. The following figures depict only the MC variant with both modal controllers activated.
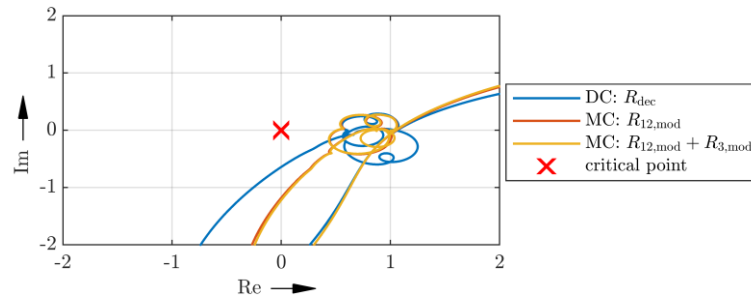

Fig. 17. BSD feed axis with two motors, velocity loop: Nyquist plot of $\det(\boldsymbol{I} + \boldsymbol{GR})$

Due to the higher gains in the velocity control loop, the reference and disturbance behaviour of the axis is slightly improved, as can be seen from Fig. 18.
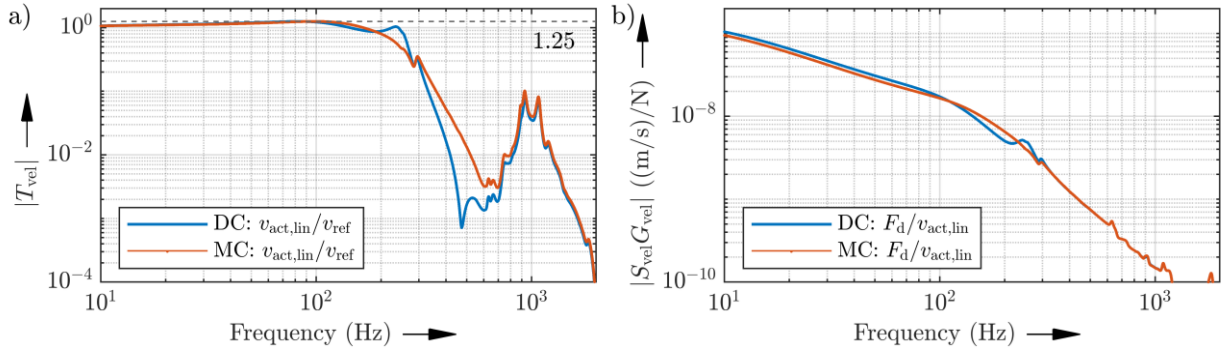

Fig. 18. Feed axis with two motors, velocity loop: complementary sensitivity function (a) and disturbance response (b)

As shown in Fig 19, modal control of the feed axis with a ball screw driven by two motors enables an expansion of the position loop control bandwidth by up to 20 %.
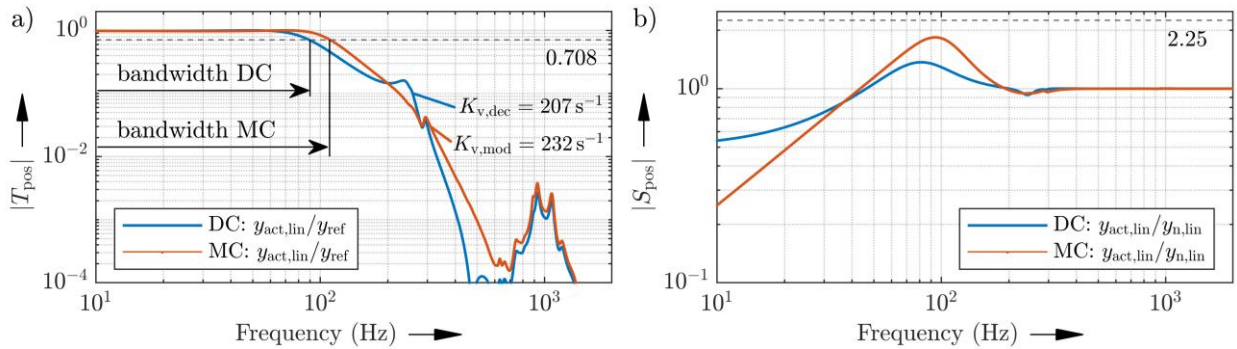

Fig. 19. Closed position loop: complementary sensitivity function (a) and sensitivity function (b)

6. CONCLUSION AND OUTLOOK

This paper has presented control strategies for ball screw-driven feed axes equipped either with an active damping device or with two motors per spindle, implemented in modal space. Applying the modal decoupling technique enables the system's eigenmodes to be controlled individually. This facilitates efficient parameterisation of the control laws, providing physical interpretability by treating vibration phenomena separately in the form of modes. The proposed controller designs for over-actuated ball screw drives improve both positioning accuracy and disturbance rejection capability. For the ball screw axis with an active damping device, the position control bandwidth can be expanded by up to 60 %. For the ball screw axis driven by two servomotors, the control bandwidth can be increased by up to 20 %.

The proposed control strategies require experimental verification. Future research will focus on developing extended modal control approaches, such as modal feedforward control.

ACKNOWLEDGEMENTS

SUPPLEMENTARY MATERIALS

The dataset associated with this publication can be accessed via https://doi.org/10.5281/zenodo.16441434 or upon request from the corresponding author.

REFERENCES

[1]   HIRAMOTO K., HANSEL A., DING S., YAMAZAKI H., 2005, A Study on the Drive at Center of Gravity (DCG) Feed Principle and its Application for Development of High Performance Machine Tool Systems. CIRP Annals – Manufacturing Technology 54/1, 333-336, https://doi.org/10.1016/S0007-8506(07)60116-4.

[2]   PÖHLMANN P., PEUKERT C., MERX M., MÜLLER J., IHLENFELDT S., 2020, Compliant Joints for the Improvement of the Dynamic Behaviour of a Gantry Stage with Direct Drives, Journal of Machine Engineering, 3, 17–29, https://doi.org/10.36897/jme/127103.

[3]   MATYSKA V., 2014, Both-Side Drive of a Ball Screw Feed Axis - Verification of the Theoretical Assumptions, Journal of Machine Engineering, 4, 29-41.

[4]   Nidec Machine Tool Corporation: Large Precision Machines MVR-Fx series, available: www.nidec.com/en/machine-tool/products/B700/M102/S100/NMTJ-mvrfx-series (accessed: 3 May 2025).

[5]   KLEINWORT R., HERB J., KAPFINGER P., SELLEMOND M., WEISS C., BUSCHKA M., ZÄH M.F., 2021, Experimental Comparison of Different Automatically Tuned Control Strategies for Active Vibration Control, CIRP Journal of Manufacturing Science and Technology, 35, 281–297, https://doi.org/10.1016/j.cirpj.2021.06.019.

[6]   ALTINTAS Y., VERL A., BRECHER C., URIARTE L., PRITSCHOW G., 2011, Machine Tool Feed Drives, CIRP Annals, 60/2, 779–796, https://doi.org/10.1016/j.cirp.2011.05.010.

[7]   YANG H., WANG Z., ZHANG T., DU F., 2020, A Review on Vibration Analysis and Control of Machine Tool Feed Drive Systems, Int. J. Adv. Manuf. Technol. 107, 503–525, https://doi.org/10.1007/s00170-020-05041-2.

[8]   PRITSCHOW G., 1998, A Comparison of Linear and Conventional Electromechanical Drives, CIRP Annals, 47/2, 541–548, https://doi.org/10.1016/S0007-8506(07)63241-7.

[9]   VERL A., FREY S., 2012, Improvement of Feed Drive Dynamics by Means of Semi-Active Damping, CIRP Annals, 61/1, 351–354, https://doi.org/10.1016/j.cirp.2012.03.135.

[10]   SUN Z., PRITSCHOW G., ZAHN P., LECHLER A., 2018, A Novel Cascade Control Principle for Feed Drives of Machine Tools, CIRP Annals, 67/2, 389–392, https://doi.org/10.1016/j.cirp.2018.03.004.

[11]   KAMALZADEH A., ERKORKMAZ K., 2007, Compensation of Axial Vibration in Ball Screw Drives, CIRP Annals, 56/1, 373–378, https://doi.org/10.1016/j.cirp.2007.05.087.

[12]   NEUBAUER M., BRENNER F., HINZE C., VERL C., 2021, Cascaded Sliding Mode Position Control (SMC-PI) for an Improved Dynamic Behavior of Elastic Feed Drives, International Journal of Machine Tools and Manufacture, 169, 103796, https://doi.org/10.1016/j.ijmachtools.2021.103796.

[13]   LIU H., ZHANG J., ZHAO W., 2017, An Intelligent Non-Collocated Control Strategy for Ball-Screw Feed Drives with Dynamic Variations, Engineering, 3/5, 641–647, https://doi.org/10.1016/J.ENG.2017.04.007.

[14]   PEUKERT C., PÖHLMANN P., MERX M., MÜLLER J., IHLENFELDT S., 2019, Investigation of Local and Modal Based Active Vibration Control Strategies on the Example of an Elastic System, Journal of Machine Engineering, 2, 32–45.

[15]   PEUKERT C., PÖHLMANN P., MERX M., MÜLLER J., IHLENFELDT S., 2019, Modal-Space Control of a Linear Motor-Driven Gantry System, MM Science Journal, 3285–3292, https://doi.org/10.17973/MMSJ.2019_11_2019083.

[16]   MEIROVITCH L., 1990, Dynamics and Control of Structures, John Wiley & Sons.
[17]   MEIROVITCH L., BARUH H., 1985, The Implementation of Modal Filters for Control of Structures, Journal of Guidance, Control, and Dynamics, 8, 707–716, https://doi.org/10.2514/3.20045.
[18]   ZÄH M.F., OERTLI T., MILBERG J., 2004, Finite Element Modelling of Ball Screw Feed Drive Systems, CIRP Annals 53/1, 289–292, https://doi.org/10.1016/S0007-8506(07)60700-8.
[19]   SKOGESTAD S., POSTLETHWAITE I., 2005, Multivariable Feedback Control: Analysis and Design, John Wiley & Sons.
[20]   SHIRVANI H.K., ZENG J.Q.C., ERKORMAZ K., 2022, Dynamic Compliance Attenuation in Ball Screw Drives Through Model-Based Active Damping of Multiple Vibration Modes, CIRP Annals. 71, 373–376, https://doi.org/10.1016/j.cirp.2022.04.040.
[21]   MEIROVITCH L., BARUH H., ÖZ H., 1983, A Comparison of Control Techniques for Large Flexible Systems, Journal of Guidance, Control, and Dynamics, 6/4, 302–310, https://doi.org/10.2514/3.19833.
[22]   BRECHER C., WECK, M., 2022, Machine Tools Production Systems 3: Mechatronic Systems, Control and Automation, Springer.